

6.1.5. Variation in Nitrate

6.1.5.1 Woe Anloga Area

Nitrate concentration varied between 0 and 754.2 mg/l in the Woe Anloga area within the period under reference. Three exceptionally high values of nitrate were observed in the Woe-Anloga Area. These include the stations at AL 7 (754.2mg/l), WE20 (449.4 mg/l) and WE2 (336.1 mg/l) high (Fig. 6.7). The first two values are associated with February and April while the third one is associated with the May 2004 measurements. Generally, conditions are better in the Woe area compared to Keta with respect to nitrate. The dry season values are high, indicating that concentration due to evaporation has occurred.

The measurements for February 2004 and April 2004 have shown the highest values recorded above. In general the nitrate concentration of the ground waters is poor and as such the shallow ground water source is not suitable for potable purposes. Agricultural activities and poor waste management practices are responsible for the current state of affairs. It must however be emphasised that in this area on the average 26 samples representing 56 % of all samples taken had nitrate levels below 10mg/l. It is also worth noting that whereas in the August and October campaigns there were 22 and 10 wells respectively without nitrate, subsequently, there was some nitrate in all the wells sampled.

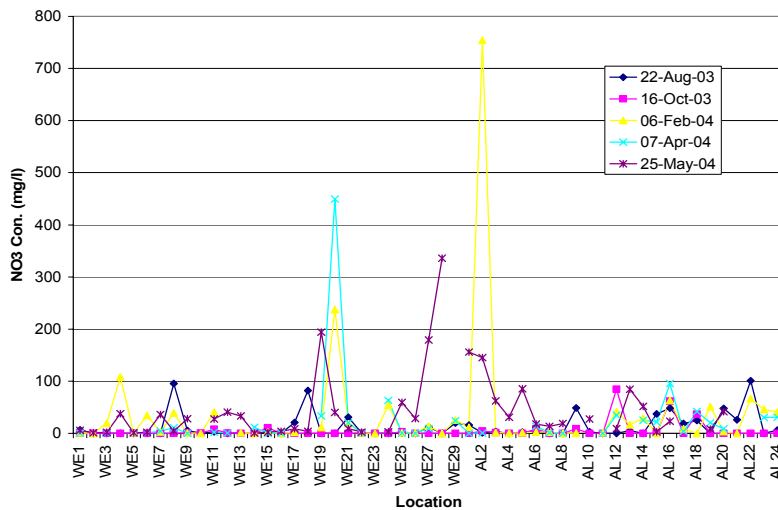


Fig. 6.7 Variation of nitrate with time and space in the Woe-Anloga area

6.1.5.2 Keta Area

In the Keta area, the concentration of nitrate varied between 0 and 567.8 mg/l. Two exceptionally high occurrences were observed from the data at K12 and KK7 (Figure 6.10). The highest value of 567.8 mg/l at Ket12 occurred in the rainy season (October 2003). This could be typical of dissolution and collection of organic matter as a result of surface runoff following rainfall events.

On the other hand the high values observed in the dry season (February and April) at KK7 (447.8 mg/l), KK33 (294.1 mg/l) could be associated with point sources which get concentrated in the dry season. (Fig. 6.8)

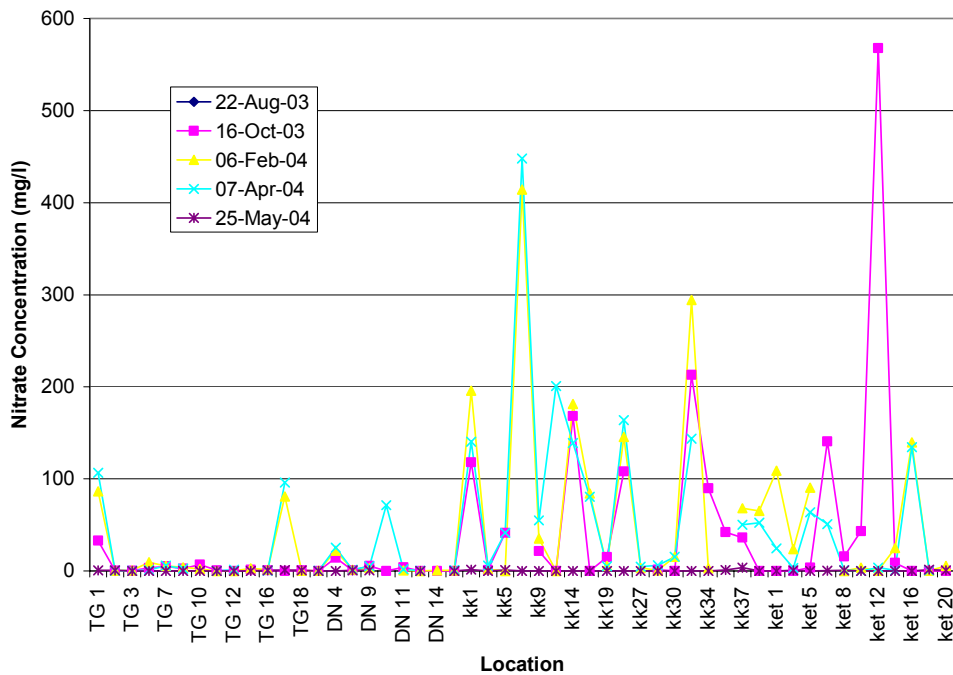


Fig. 6.8 Variation of nitrate with space and time in the Keta area

6.2. Hydrochemistry of Groundwater In The Keta And Anloga Areas

The water quality parameters presented in the previous sections indicate that water in both the Keta and the Woe-Anloga area fall short of the required standards for drinking

water set by the WHO. A study of the hydrochemistry of the water in these areas also serves to establish the chemical character of the water in the study area indicating the probable processes that have occurred.

The hydrochemical facies classification using both the Piper Trilinear and Durov diagrams are also shown Figs. 6.9 and 6.10 respectively. It must be stated that similar plots for Woe-Anloga yielded the same results and therefore need not be represented.

The main water types are the $\text{Ca}^{2+} \text{Na}^+\text{HCO}_3^-\text{Cl}^-$, Na^+Cl^- , $\text{Ca}^{2+} \text{HCO}_3^-$ and $\text{Na}^+\text{HCO}_3^- \text{Cl}^-$ types. The hydrochemistry is dominated by the first two water types and all but one does not have dominant bicarbonate ions and bearing in mind that the aquifer is dominated by sand, the likely source of the bicarbonate is carbon dioxide in the atmosphere and soil vapour. Chloride ions appear to have over-riding dominance and reflect strongly in the Durov diagram (Fig. 6.10)

Fig. 6.9 Piper Trilinear diagram of the Keta area showing groundwater types in the area

Fig. 7.10 Durov plot of groundwater parameters for the Keta area

The Durov plot indicates strongly end-point waters characterized by $\text{Na}^+ \text{Cl}^-$. The plot also depicts significant recharge, ion exchange, and mixing processes during the circulation of the groundwater.

6.3 Geophysical Investigations

The geophysical investigations were employed to delineate formations bearing fresh and saline water, distinguish between sandy and clay layers and establish the depth to the freshwater-saline water interface. The geophysical techniques used in this investigation were the Schlumberger resistivity profiling and sounding methods, the theory of which is beyond the scope of this report.

This section discusses the results of the borehole-controlled VES, where the layer resistivities were superimposed on the borehole lithologic logs. As a result, the project area has been divided into two main sections based on the geology. The area that stretches from the Anloga-Keta road towards the Keta lagoon is referred to as the northern sector and is underlain basically by the lagoon clays and where the sand layer is less than 3 m thick. The area, which stretches from the Keta-Anloga road to the Gulf of Guinea coast, including the intervening depressions is referred to as the southern sector and primarily underlain by the marine sands (Fig.6.11).

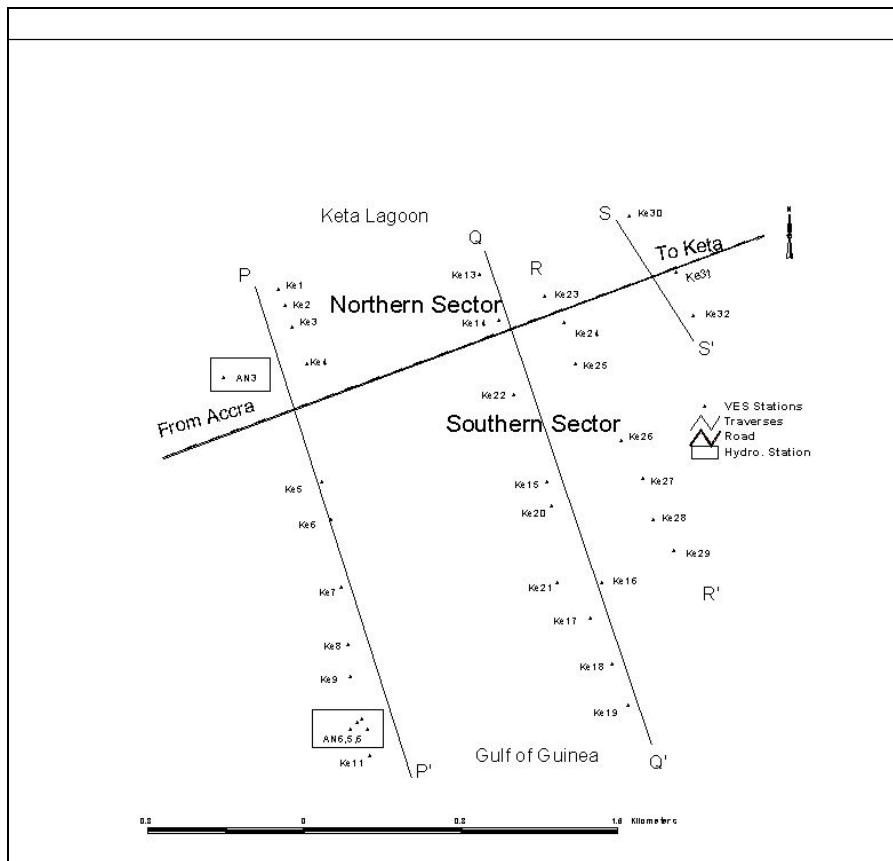


Fig. 6.11 Map showing the division of the area into two geological and/or hydro-geophysical sectors

Vertical electrical sounding was carried out to establish the distribution of saline aquifers in the area used as pilot study. The Schlumberger configuration was used in carrying out the vertical electrical sounding.

Modeling of VES results was carried out using the softwares RESIST and IPmin, both of which are iterative inversion-modeling programs. Analysis of the resulting apparent resistivity versus the half-current electrode separations yielded layered earth models composed of individual layers of specified thickness and apparent resistivity.

Basically the area is underlain by a four-layer structure. The VES results (apparent resistivity and thickness) were used to construct interpretative vertical iso-resistivity cross-sections along traverses PP¹ and QQ¹. Tables 6.2 and 6.3 are a summary of results of resistivity models for all sounding points during the wet and dry seasons.

Table 6.2 Summary of results from computer modeling (resist) for all sounding points during the wet season.

VES Stations	No. Of Layers	Resistivity of layers (Ohm-m)					Thickness of Layers (m)			
		ρ_1	ρ_2	ρ_3	ρ_4	ρ_5	T ₁	T ₂	T ₃	T ₄
KETA B1	4	0.6	4.3	1.3	0.1		4.5	12.4	69.6	
KETA B2	4	0.6	17.3	1.7	0.1		2.7	8.4	70.4	
KETA B3	3	2.4	32.7	2.1			0.9	12.9		
KETA B4	2	1.5	7081				0.9			
KETA B5	4	1436.9	3322.5	101	10.9		1.2	3.0	17.2	
KETA B6	4	865.4	712.7	7.8	11.7		9.2	0.5	231.6	
KETA B7	4	61.4	107.3	10.9	33.9		5.8	6.5	18.4	
KETA B8	5	113.5	2832.0	5.0	13.5	1111.1	0.6	1.6	9.6	8.7
KETA B9	5	87.2	27.6	46.7	3.1	0.9	1.5	1.5	18.7	7.6
KETA B10	5	1206.0	2964.2	57.5	2.7	2524.5	1.5	1.1	13.8	23.4
KETA B11	4	1058.8	7618.3	56.0	25.3		0.4	1.4	50.3	
KETA B12	4	60.3	3337.1	12.8	10.6		0.4	2.1	16.5	
KETA B13	4	2.9	1.3	7.5	1.0		3.0	4.7	14.1	
KETA B14	4	32.4	29.1	5.3	1.7		1.3	23.0	1.0	
KETA B15	5	8345.8	193.9	67.9	106.5	0.2	3.8	7.0	154.3	9.1
KETA B16	4	2215.8	55.9	35.0	3.7		1.2	6.6	12.1	
KETA B17	3	853.7	48.0	0.7			1.2	21.1		
KETA B18	4	53947.9	135.7	7.3	412.3		0.9	5.8	86.9	
KETA B19	5	14741.2	4845.5	20.9	7.4	1175.4	0.5	2.1	10.5	42.2
KETA B20	4	15702.9	91.5	107	366.9		2.1	4.0	115.9	
KETA B21	5	1371.6	75.7	21.9	3.1	38.5	0.6	10.5	22.7	21.7
KETA B22	5	5998.7	5673.8	19.6	1.7	18.5	1.8	0.5	11.9	7.1

Table 6.3 Summary of results of resistivity modeling conducted for all sounding points during the dry season.

VES Stations	No. Of Layers	Resistivity of layers (Ohm-m)					Thickness of Layers (m)			
		ρ_1	ρ_2	ρ_3	ρ_4	ρ_5	T_1	T_2	T_3	T_4
Keta A01	4	0.1	7.3	1.3	11.3	-	2.1	13.4	54.4	-
Keta A02	4	0.7	26.5	19.5	1.6	-	2.8	7.8	1.5	-
Keta A03	4	3.7	3.9	8.2	1.9	-	2.2	0.8	17.6	-
Keta A04	3	79.2	18.4	2.1	-	-	3.5	30.4	-	-
Keta A05	5	514.8	1669.5	38.4	2.2	5634	0.5	3	11	4.5
Keta A06	5	1938	6452	342.3	12.5	29.8	0.2	3.3	7.5	117
Keta A07	3	3467.6	111.6	1.6	-	-	2.91	14		-
Keta A08	4	221.7	7813.7	107	4.3	-	0.5	1.4	2.7	-
Keta A09	5	92.3	39.4	184.6	18.3	1.8	0.6	1.7	3.4	28.6
Keta A10	4	341.8	803.9	50.2	4.1	-	0.8	2.8	12.7	-
Keta A11	5	104.2	3.0	0.9	9.1	0.5	3.4	23.9	9.4	69.5
Keta A12	4	60.3	3337.1	12.8	10.6	-	0.4	2.1	16.5	-
Keta A13	4	3.4	1.7	6.2	0.4	-	1.1	5.6	40.1	-
Keta A14	5	105.6	109.8	23.6	5.2	334.4	3	0.4	16.2	84
Keta A15	3	24876	21.3	10000	-	-	3.2	58.3	-	-
Keta A16	4	421.2	37.8	2	3257	-	3	13.7	37.8	-
Keta A17	4	188	56.7	0.1	334	-	2.1	12.4	18.7	-
Keta A18	5	10451	6077.1	67.1	10.9	373.2	0.3	1.6	8.4	30.4
Keta A19	6	1824.7	65.1	8.0	1.7	34.9	3.6	0.9	14.1	18.2
Keta A20	4	9791.1	298.1	24.8	32.4	-	2.9	8.8	55.9	-
Keta A21	5	1371.6	75.7	21.9	3.1	38.5	0.6	10.5	22.7	21.7
Keta A22	5	5998.7	5673.8	19.6	1.7	18.5	1.8	0.5	11.9	7.1

6.3.1 Calibration Of Boreholes With Geophysical Data

The sounding results were calibrated using test boreholes drilled in the vicinity of the sounding points. The results were used to adopt certain ranges of apparent resistivity values to indicate the zones of saline water aquifers, thick clay layers, freshwater aquifers and desiccated layers.

The layer resistivities and thicknesses for the soundings carried out on each borehole were superimposed on the lithologic logs of the test boreholes. However, the fact that the same materials and rock types were encountered especially at shallow depths at each drilling site, the deepest test boreholes at each site were used in the text for the discussions. The layer resistivities and thicknesses for all the calibration curves are summarized in Table 6.4. The integrated lithological and sounding results from the two drilling sites are shown (Fig.6.12 and Fig. 6.14) and these figures are representative of hydrogeophysical conditions pertaining in the northern and southern sectors respectively.

Table 7.4 Summary of resistivity model results for all sounding stations during the borehole calibration/characterization

VES Stations	No. Of Layers	Resistivity of layers (Ohm-m)						Thickness of Layers (m)				
		ρ_1	ρ_2	ρ_3	ρ_4	ρ_5	ρ_6	T_1	T_2	T_3	T_4	T_5
4LAN13EW	4	22.7	8.2	32.2	0.2	-	-	6.2	4.7	9.6		
5LAN13EW	5	22.7	7	29.8	26	0.2	-	6.3	3.7	7.2	4	
AN13NS	5	21.8	26	10.4	22.7	4.3	-	0.5	3.2	3	10	
4LAN4EW	4	2257.7	53.6	2.7	71.2	-	-	2.1	13.1	6.9		
5LAN4EW	5	2258.5	2715.3	54.2	5	57.9	-	1.9	0.1	12.6	12	
AN4NS	4	1955.8	7056.6	79	15.5	-	-	0.6	0.6	7.9		
AN5NS	4	2158.5	75.1	10.4	50.1	-	-	1.1	7	8.5	4.3	
AN5EW	4	3188.1	91.7	17.8	428.6	-	-	1.2	7.9	28.1		
AN6NS	5	365.8	1685.3	38.2	4.5	253.9	-	0.4	0.9	12.3	18	
AN6EW	6	306.8	1259.4	22.8	97.7	5.8	334	0.5	0.9	2.4	6.8	21

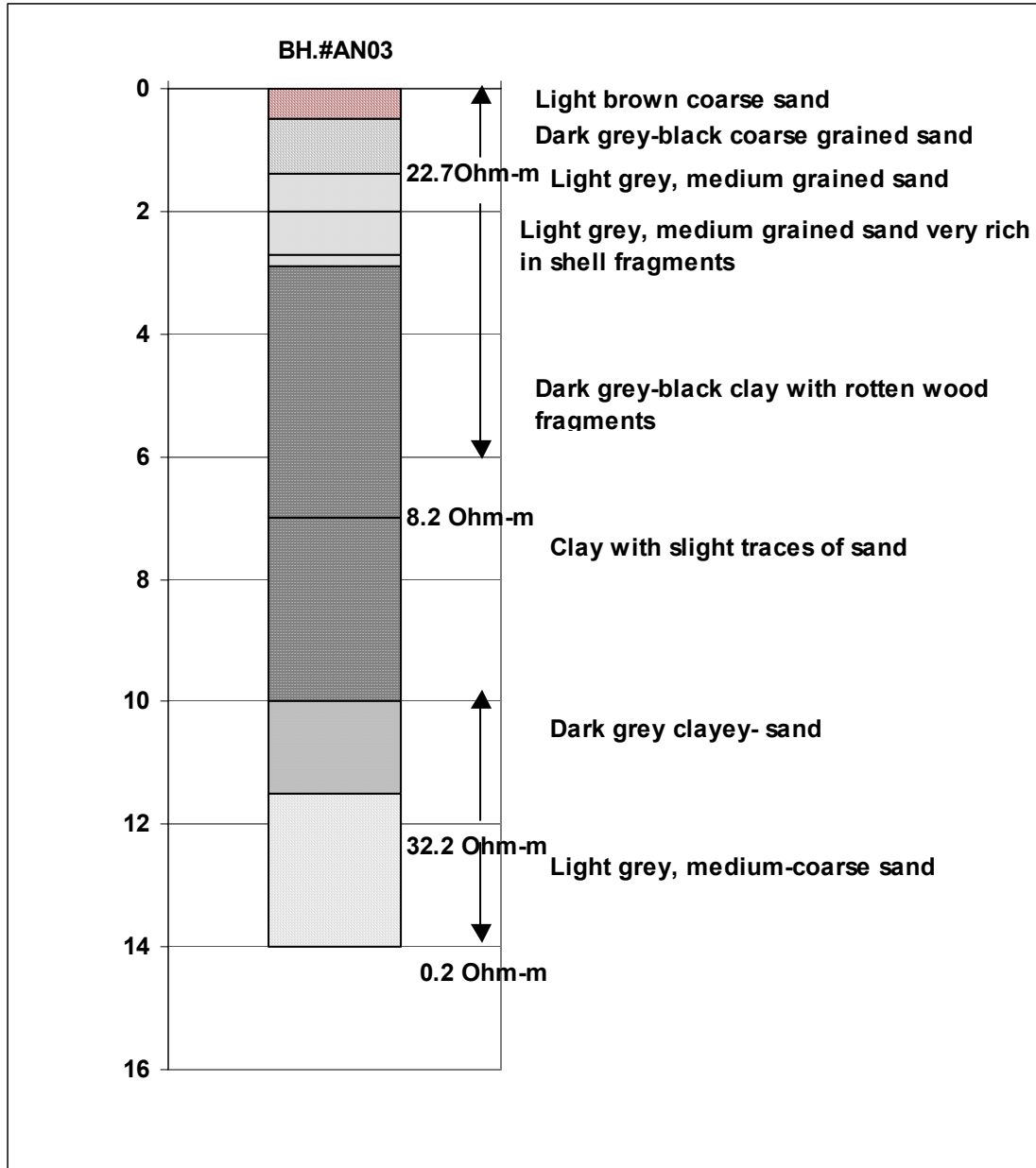


Fig. 6.12 A representative composite lithological log with subsurface superimposed layer resistivities (northern sector)

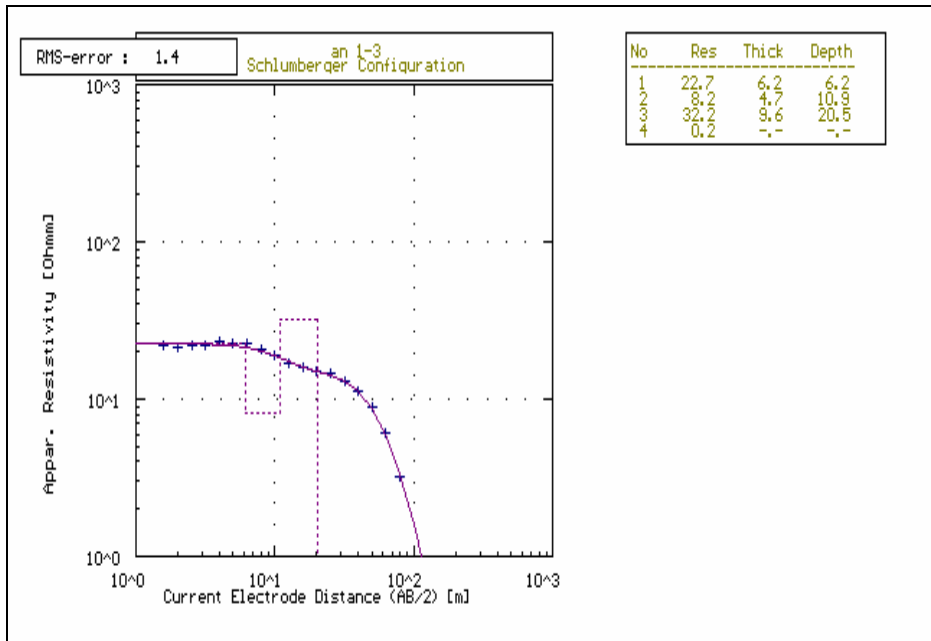


Fig. 6.13 A VES modeled curve for the borehole soundings in the northern sector.

Results of the VES conducted for the test wells AN1, AN2 and AN3 indicate that the northern sector is basically underlain by a four-layer structure (Fig. 6.13). The top layer has an average apparent resistivity of 27.1 Ohm-m and an average thickness of 6 m. The second layer has resistivity of 8.2 Ohm-m and a thickness of 4 m. The third layer has resistivity of 32 Ohm-m and is 8.2 m thick. The infinitely thick bottom layer has an apparent resistivity of 0.2 Ohm-m. Correlating this with the drilling results, the top layer is mainly medium to coarse sand. On the whole, the top layer resistivity is comparatively low in this northern sector and could be due to partial saturation of the sand caused by continuous irrigation in the area. The high organic and inorganic fertilizer concentrations could also account for such low resistivities. The second zone corresponds to the relatively thick sandy-clay. The third layer is medium to coarse freshwater sand aquifer. Drilling was not extended beyond 14 m at this sector. However, based on the analyses of lithologic logs of other water supply boreholes in the area and also geological, hydrogeological and field observations, it was confirmed that the extremely low resistive bottom layer is a thick layer of clay probably saline-saturated.

Similarly, Figures 6.14 and 6.15 represent the modeled VES results and the composite VES/lithologic graphs respectively for the test wells AN4, AN5, and AN6 located near the Gulf of Guinea coast.

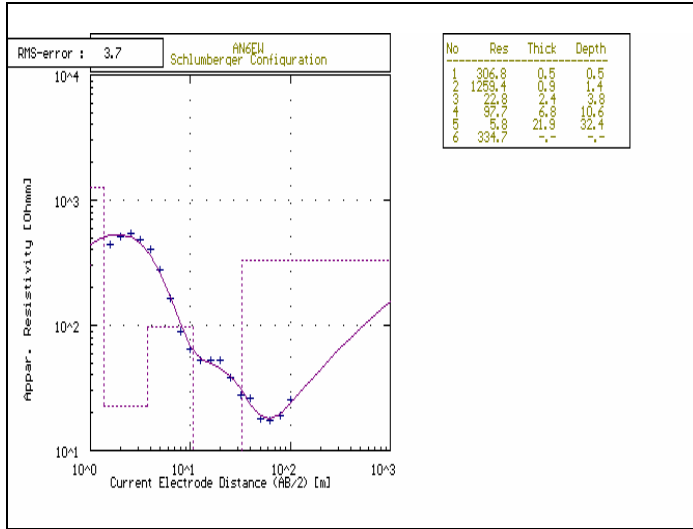


Fig. 6.14 A VES modeled curve for the borehole sounding in the southern sector